A hybrid transfer function procedure for broadband auralization within small flight vehicle interiors

Albert R. Allen[1]
Siddhartha Krishnamurthy[2]
NASA Langley Research Center
Hampton, VA 23681, USA

ABSTRACT

Auralization of the sound fields within flight vehicle interiors is of interest to aircraft designers considering crew and passenger ride quality. Computer models can be used to predict the filtering effects that the fuselage structure and interior volume have on the exterior sound field in order to simulate the resulting cabin interior noise. However, this can become expensive when a wide frequency range of analysis suitable for passenger auralization is desired. This is particularly the case when using deterministic modeling methods such as finite element analysis (FEA) wherein prohibitively high levels of detail and finite element discretizations are required to resolve the wavelengths at high frequencies. On the contrary, Statistical Energy Analysis (SEA), while not capturing important modal behaviors at low frequencies, is better suited for higher frequency analyses where structural and interior dynamics exhibit high modal overlap and spatially averaged physical quantities suffice. For this reason, a hybrid procedure is considered here that utilizes FE modal solutions at lower frequencies and SEA results at higher frequencies. A transfer function dataset containing the exterior to interior vibroacoustic filtering effect is calculated accordingly and subsequently stored to be used for a variety of exterior dynamic load cases. At low frequencies, the transfer function dataset detail is related to the level of FE model refinement whereas at high frequencies it functions as an equalizer array with a level of detail corresponding to the SEA subsystem partitioning scheme. The above procedure is described herein and demonstrated on a six-passenger flight vehicle with eight propulsors in a hover flight condition.

1. INTRODUCTION

The National Aeronautics and Space Administration (NASA) Revolutionary Vertical Lift Technology (RVLT) Project is developing tools and strategies to assess ride quality and address noise issues inherent to new multi-rotor Urban Air Mobility (UAM) vehicles. The ability to produce sound field

[1]albert.r.allen@nasa.gov

[2]siddhartha.krishnamurthy@nasa.gov

auralizations within flight vehicle interiors aligns with the RVLT Project goals and is of interest to aircraft manufacturers evaluating design decisions in terms of the crew and passenger sound experience. Auralizations have often been informed by flight recordings. For example, flight recordings were used by Powell and Sullivan to evaluate active noise control treatments in propeller driven airplanes [1]. However, because most UAM vehicle concepts are still in the early stages of development, interior noise flight recordings of UAM vehicles are not yet widely accessible. It would be advantageous to be able to hear the noise inside novel flight vehicle cabins through simulation before those vehicles are flight ready. The acoustic ramifications of design decisions could then be *listened to* by interested parties, and noise problems could be made evident in the early phases of design before major capital expenditures.

Important noise sources relevant to UAM vehicles are the acoustic field radiating from propulsors, flow induced fluctuating pressure fields such as the turbulent boundary layer, and mechanical sources emanating from the drive train or other internal mechanisms. The fuselage structure and interior acoustic volume act as a filter that modulates these excitations depending on their location and transfer path to interior listener points. Computer models may be used to simulate the filtering effect between any given source and receiver pair, thus creating a transfer function dataset representing the fuselage and interior vibroacoustic system. Likewise, dynamic excitations relevant to flight vehicles can be simulated and applied to the transfer function dataset. Given the frequency range of human hearing, transfer functions spanning a broad range of frequencies are desired for adequate auralizations. The difficulty lies with development of a transfer function dataset that describes the vehicle vibroacoustic system dynamic behavior over a broad range of frequencies. In order to accommodate a variety of dynamic load cases, it must also be able to accept one or a combination of excitation fields. Ideally, changing the dynamic loading would not necessitate changing the transfer function dataset, and for typical use cases the two components could be dealt with independently. Finally, the procedure should utilize readily available computational modeling techniques with flexibility in terms of simulation fidelity.

Consequently, a hybrid, low frequency (LF) and high frequency (HF) procedure utilizing the Finite Element Method (FEM) and Statistical Energy Analysis (SEA) has been considered. Given adequate FE resolutions and modeling detail, the FEM is capable of describing the LF vehicle dynamic behavior with high spatial detail, including modal interactions and point-to-point phase relationships. At HFs, however, prohibitively high levels of modeling detail and FE discretizations are required to resolve the smaller wavelengths. In other words, the FEM becomes intractable both in terms of model building and solve times required to compute the deterministic, phase-accurate response at higher frequencies. It can be argued that *deterministic* modeling methods such as the FEM will *generally* tend to suffer from phase inaccuracies at HFs due to the inability of the modeler to specify adequate modeling details at the smaller scales required for HF analysis in complex, realistic vibroacoustic systems. SEA is better suited for HF analyses where structural and interior dynamics exhibit high modal overlap and spatially averaged physical quantities suffice. However, with SEA, phase information is lost and important modal interactions are not captured, thus making it a poor choice at LFs. With the hybrid procedure considered here, the transfer function dataset detail is related to the FE model fidelity at LFs, whereas it functions as an equalizer array with a level of detail corresponding to the SEA subsystem partitioning scheme at HFs.

In the following, the hybrid procedure is described and exercised on NASA RVLT's six-passenger vertical takeoff and landing (VTOL) Lift + Cruise (L+C) concept, a baseline design suitable for UAM transportation [2]. The transfer function dataset containing the exterior to interior vibroacoustic filtering effect is calculated using LF and HF modeling techniques. Following this, the dynamic

pressure field emanating from the eight propulsors rotating in a hover flight condition is applied to the vehicle exterior and resulting pressure time histories are simulated in the interior.

2. PROCEDURE

A three-dimensional linear vibroacoustic system including an interior acoustic volume Ω_a enclosed by an elastic structure Ω_s is considered here, as shown in Figure 1. A surface-normal harmonic point force f_m acting on the exterior surface of the structure at $r'_m = (x'_m, y'_m, z'_m)$ produces a steady-state dynamic velocity field $v(\mathbf{r}')$ at positions $\mathbf{r}'$ in Ω_s. The surface-normal velocities are $v_{z'}$ in the local coordinates $\mathbf{r}' = (x', y', z')$. The structural velocity field couples with and radiates into the interior acoustic volume producing steady-state dynamic pressure p_k at listener locations r_k. While inplane components $v_{x'}$ and $v_{y'}$ contribute to overall structural dynamics in complex structures, only the surface normal component couples efficiently to the interior acoustic volume, which motivates the specification of surface normal components.

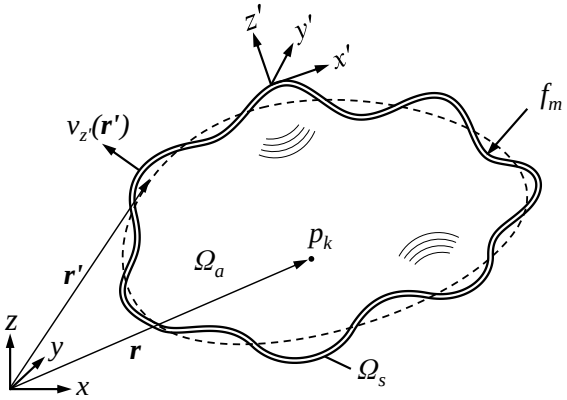

Figure 1: A three-dimensional vibroacoustic system.

By assuming a unit normal input force f_m at all points of interest along $\mathbf{r}'$ and solving, separately for each f_m in $\mathbf{f}$, for the resulting interior response spectra at each listener location of interest p_k in $\mathbf{p}$, a frequency domain transfer function dataset $\mathbf{H}$ of the form

$$H_{m,k} = \frac{p_k}{f_m} \tag{1}$$

can be developed (spectral dimension implied). For a given discretized finite spectral size N_f, $m = 1, \ldots, M$ excitation points, and $k = 1, \ldots, K$ listener locations, the resulting transfer function dataset has dimension $N_f \times M \times K$. Excitations X_m consisting of fluctuating pressure fields, localized forces, or combinations thereof can then be applied within the set of M excitation points considered in $\mathbf{H}$ to calculate resulting pressure spectra at listener locations $\mathbf{p}$ by multiplying in the frequency domain as

$$Y_{m,k} = H_{m,k} X_m. \tag{2}$$

Time histories at listener locations are then produced by applying the inverse Fourier transform and summing over the M excitation points as

$$y_k(t) = \sum_M \left(\frac{1}{2\pi} \int_{-\infty}^{\infty} Y_{m,k} e^{-j\omega t} \, \mathrm{d}\omega \right). \tag{3}$$

Equation 3 is readily carried out using commonly available FFT implementations.

The procedure described above serves as a summary of the procedure carried out in practice. Also considered, but not described here, are additional signal processing pre- and post-conditioning steps that can be taken to arrive at serviceable auralization time histories. These are specific to a given application and could include reconstructing the two-sided complex conjugate spectra, interpolation, fading, stitching, blending, artifact removal, etc. In terms of computational expense, the effort largely pertains to populating the transfer function matrix $\mathbf{H}$ by solving for p_k for each f_m. The computational expense of determining the excitation X_m may also be significant, but will vary depending on the application and is not the main focus here. A variety of techniques exist to solve for the response of linear vibroacoustic systems excited dynamically. Two methods considered here are the FEM and SEA, which have been extensively developed and are frequently accessible in terms of user knowledge and software as opposed to more specialized or esoteric analysis techniques.

2.1. Finite Element Analysis Component

The direct steady-state dynamic FE solution entails the calculation of the response p_k due to f_m directly in terms of the physical degrees of freedom of the model. This method is particularly suited for cases involving strong structural-acoustic coupling effects, frequency dependent damping, or propagation through localized regions of damping such as porous acoustic media. For situations where overall structural and acoustic system damping specifications suffice and where structural dynamics are not strongly influenced by the presence of the coupled acoustic region and vice-versa, the response can be calculated more efficiently in a mode-based steady-state dynamic analysis subsequent to individual modal decompositions of the structure and acoustic volume. The latter approach is used here. Modal decompositions of the undamped in-vacuo structural (Ω_s) and undamped hardwall acoustic (Ω_a) systems are computed by solving the eigenvalue problem of the form $\left(-\omega^2\mathbf{M} + \mathbf{K}\right)\psi = 0$, where $\mathbf{M}$ and $\mathbf{K}$ denote the mass and stiffness matrices of the associated FE system. The orthogonal structural eigenvectors $\psi^s = \left(\psi_0^s, \psi_1^s, \ldots, \psi_n^s\right)$ and eigenfrequencies $\omega^s = \left(\omega_0^s, \omega_1^s, \ldots, \omega_n^s\right)$ can be determined using a FE solver utilizing the Lanczos or other applicable algorithm. This is repeated for the acoustic system to obtain ψ^a and ω^a.

With structural modes ψ^s, a matrix of surface normal velocity response spectra of size $N_f \times M \times M_w$ including the velocity response spectra at all points $m_w = 1, \ldots, M_w$ wetted to the interior volume due to unit point forces f_m at the M excition points is calculated using a frequency response summation

$$v\left(\mathbf{r}'_m, \mathbf{r}'_{m_w}\right) = \sum_{n=0}^{N^s} \frac{j\omega f_m}{\omega^2 - {\omega_n^s}^2} \psi_n^s\left(\mathbf{r}'_m\right) \psi_n^s\left(\mathbf{r}'_{m_w}\right). \tag{4}$$

Here, $\omega = 2\pi f$ and N^s is the number of structural modes included, which corresponds with the frequency range of analysis. In Equation (4), the spectral dimension of v is implied, and the eigenvectors ψ_n^s are scaled such that the generalized mass for each vector is unity. Complex eigenfrequencies may also be incorporated here to account for small modal damping by substituting $\omega_n^{s*} = \omega_n^s(1 + j\zeta)$, where ζ is the modal damping ratio. It is worth noting here that significant or

localized damping will not be represented well by this simplistic damping model and may require a complex eigensolution or direct steady state dynamic solution to populate $v\left(\mathbf{r}'_m, \mathbf{r}'_{m_w}\right)$.

Following Koopman [3], the pressure response at interior listener locations $\mathbf{r}_k$ due to a volume velocity source Q located on the structural-acoustic coupled surface along $\mathbf{r}'$ are then determined using the Green's function for an enclosed acoustic space $\mathbf{G}\left(\mathbf{r}_k, \mathbf{r}'_{m_w}\right)$ by

$$p\left(\mathbf{r}_k, \mathbf{r}'_{m_w}\right) = j\omega\rho_0 c_0^2 Q\left(\mathbf{r}'_{m_w}\right)\mathbf{G}\left(\mathbf{r}_k, \mathbf{r}'_{m_w}\right), \tag{5}$$

where ρ_0 and c_0 are the density and speed of sound in Ω_a. Equation 5 requires a coordinate transformation between $\mathbf{r}$ and $\mathbf{r}'$. In a FE context, Q may be formulated as the surface normal velocity at a given node multiplied by the corresponding nodal area. The Green's function in the enclosure is given as

$$\mathbf{G}\left(\mathbf{r}_k, \mathbf{r}'_{m_w}\right) = \sum_{n=0}^{N^a} \frac{\psi_n^a\left(\mathbf{r}'_{m_w}\right)\psi_n^a\left(\mathbf{r}_k\right)}{V_n}\left(\frac{\omega_n^{a2} - \omega^2 - j\omega\eta_n^a\Delta\omega_n^a}{\left(\omega_n^{a2} - \omega^2\right)^2 + \left(\omega\eta_n^a\Delta\omega_n^a\right)^2}\right), \tag{6}$$

where V_n are the modal volumes of the cavity. Interior damping is, in keeping with the formulation in [3], accounted for by the modal half-power bandwidth $\Delta\omega_n^a$.

2.2. Statistical Energy Analysis Component

SEA, a high frequency vibroacoustic prediction technique, is used to populate $\mathbf{H}$ at higher frequencies. SEA considers the energy transfer between resonant modes within subsystems. The complex matrix equations describing the vibroacoustic behavior of the system in FE-based models are instead approximated by matrix equations that describe the vibrational power transmission between subsystems, which is dictated by subsystem impedances, subsystem interconnectedness, and energy dissipation within subsystems due to damping [4]. Exact response and phase information are lost, but energy transmission between and average responses within subsystems are predicted. The size of the problem is directly related to the number of subsystems, which leads to considerably smaller matrix sizes relative to the FEM as subsystems are typically specified as entire regions consisting of large numbers of modes. The primary variables considered in SEA are power and energy, but the transfer function $\mathbf{H}$ in Equation 1 requires pressures and forces. Fortunately, SEA variables have been formulated using mobility functions containing excitation and response variables of interest such as pressure and force [5, 6].

Briefly, the unit force f_m applied to Ω_s when developing $\mathbf{H}$ is now specified as an average RMS point force $\langle f_{rms}\rangle$ applied somewhere within a given subsystem. The subsystem input power W^{in} due to a point force becomes independent of the precise location of the force at higher frequencies. Referring to [5], by using the average conductance G, which is the real part of the mechanial mobility, a relationship between force and power is given by

$$W^{in} = \left\langle f_{rms}^2\right\rangle G. \tag{7}$$

With the force specified at a given subsystem within Ω_s, the subsystem power input is known and the system is solved to determine the resulting energies E throughout all subsystems by inverting the loss factor matrix [4]. The expected RMS pressure within the interior acoustic volume is then related to the energy by

$$E = \left\langle p_{rms}^2\right\rangle \frac{V}{\rho_0 c_0^2}. \tag{8}$$

Commercial SEA software exists that allows for the specification of excitation variables in lieu of power inputs and provides subsystem expected response variables in lieu of subsystem energy, thus simplifying the process [7].

To maintain uniformity between the low and high frequency components in $\mathbf{H}$, $\langle f_{rms} \rangle$ is *considered* the average force due to individual forces $f_{rms,m}$ distributed throughout the subsystem and applied sequentially as was done in Equation 4. In practice, however, the system is solved only once per subsystem, and resulting pressure responses $p_{rms,k}$ are associated with individual m forces by assigning unit $f_{rms,m}$ onto all m points within the subsystem, i.e. the FE nodes, and scaling to account for variations in nodal areas and situations where nodes are shared by two or more subsystems. Furthermore, a complex valued response is constructed with the reintroduction of artificial phase by

$$p_k^* = \sqrt{2} p_{rms,k} e^{j\theta}, \tag{9}$$

where θ is a random phase angle sampled within $[-\pi, \pi]$ for each m and k. For points close to the acoustic volume's boundaries, pressure spectra created in this manner might require additional level corrections to take into consideration the interference patterns near walls. [8].

In Equation 2, the excitations X_m are applied at the FE resolution, and any spatial correlations inherent to the excitation field are resolved assuming adequate excitation field and FE resolutions are maintained. However, the FE resolution may be inadequate for resolving certain correlated excitation fields above the LF to HF transition frequency. In essence, "rain on the roof" (RotR) excitations are assumed when specifying $f_{rms,m}$ here as the point force excitations applied in the SEA solver are by definition uncorrelated. Uncorrected, this results in biased response levels in the structural and acoustic subsystems if the applied excitation field deviates from uncorrelated RotR excitation. One solution for this problem is to determine a correction spectrum C^{eq} that imparts the same amount of vibration levels on the structure as a given spatially correlated excitation such that

$$\left\langle f_{rms}^2 \right\rangle = C^{eq} \left\langle f_{rms}^2 \right\rangle_{RotR}. \tag{10}$$

Ichchou has provided C^{eq} for reverberant and turbulent boundary layer excitation fields [9]. In the application described below, the reverberant excitation field correction spectrum $C^{eq} = \pi^2 c_0^2 / \omega^2$ has been applied.

3. APPLICATION

The procedure described here was carried out on a simplified version of the L+C UAM vehicle subject to acoustic excitations from eight rotors in a hover flight condition. A sketch of the vehicle is shown in Figure 2 (aft propulsion rotor is not used during hover). FE and SEA models of the vehicle are shown in Figure 3 and were developed in Abaqus CAE and VA ONE [7, 10] with a target LF to HF cutoff of 500 Hz. The fuselage skins as well as interior bulkheads were modeled using 12 layers of 0.2 mm thick carbon fabric laminas with nominal properties assumed ($E_1 = E_1 = 60$ GPa, $\nu_{12} = 0.37$, $G_{12} = 4.2$ GPa, $G_{13} = G_{23} = 3.3$ GPa, $\rho = 2408$ kg/m^3). Box-beam stiffeners were also included and were comprised of the same carbon fabric laminas with a height (skin normal) and width of 63.5 mm $\times$ 25.4 mm and a uniform wall thickness of 2.4 mm. The windshields were modeled as 10 mm thick acrylic ($E = 3$ GPa, $\nu = 0.37$, $\rho = 1200$ kg/m^3). The crew and passenger interior acoustic volume was approximately 11.5 m^3 and was modeled as standard air ($\rho_0 = 1.21$ kg/m^3, $c_0 = 343$ m/s).

The structural and acoustic portions of the FE model were developed in parallel and solved separately. The skins and frames were modeled using 8,198 second order shell (S8R) and beam (B32)

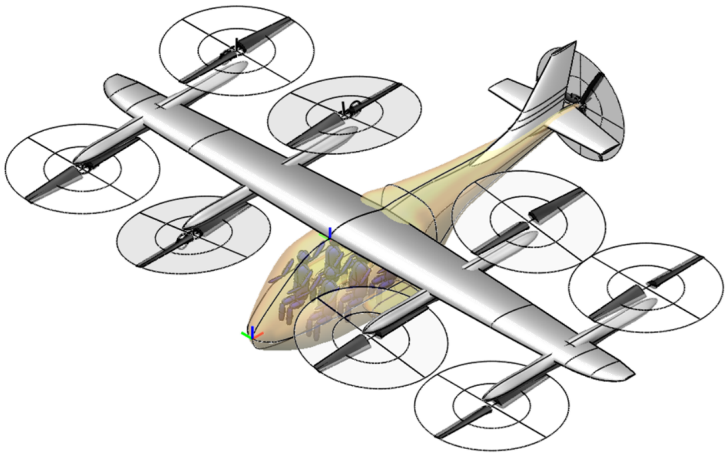

Figure 2: Sketch of the Lift + Cruise 6-seater UAM vehicle [2].

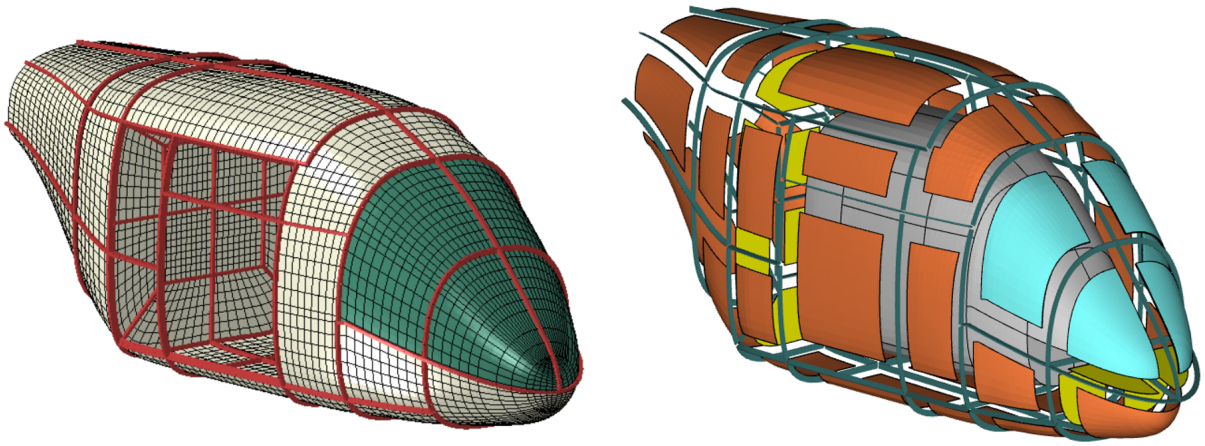

Figure 3: FE model (left) and SEA model (right) of the L+C vehicle.

elements, while the acoustic volume was comprised entirely of 30,527 second order tetrahedrons (AC3D10). The first 1,393 structural modes and 502 interior acoustic modes were extracted using the standard Lanczos eigensolver within Abaqus and stored for further post-processing. The selected sets of modes described the dynamic behavior of the structural and acoustic systems up to 500 Hz. Modes above 500 Hz were also included to account for the sub-resonant content of the neighboring out-of-band modes. The SEA model consisted of 57 shell subsystems (41 exterior facing skin subsystems and 16 internal bulkhead subsystems), 108 beam subsystems representing the stiffening frames, and one interior acoustic volume. Coupling loss factors describing the power transmission between subsystems were assigned using the standard junction assignments in VA ONE. Equivalent material properties were applied between the two models. FEM structural and acoustic modes were assigned frequency-independent damping ratios of 1% and 2.5%, respectively, while the corresponding SEA subsystems were assigned equivalent damping loss factors of 2% and 5%. As seen in Figure 3, some simplifications were made during model development. These included

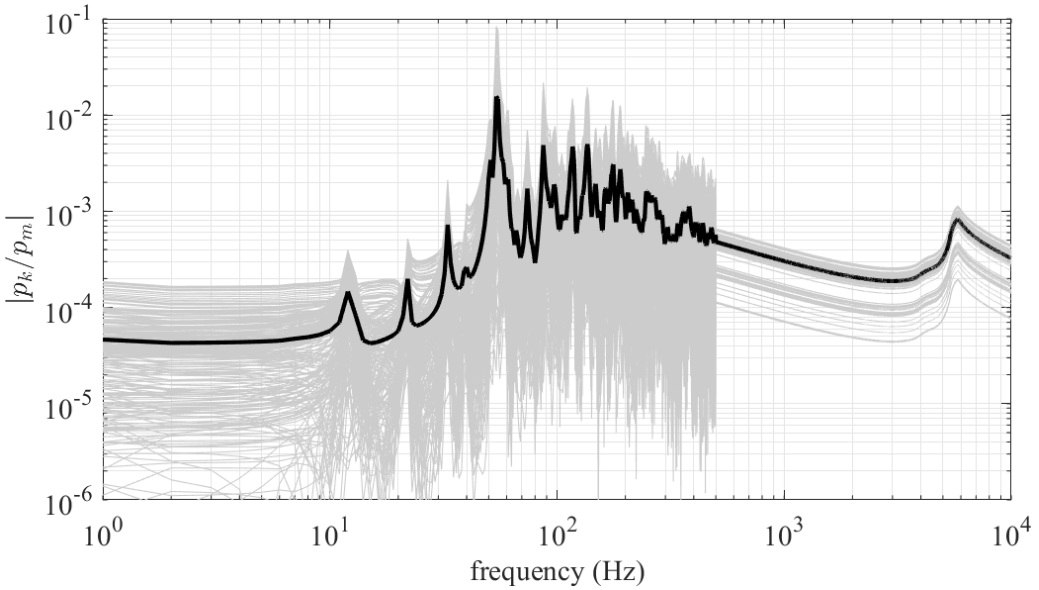

Figure 4: Spread (—) and mean value (**—**) of the components of **H** pertaining to the interior response at one location relative to 234 unit excitations along one of the side panels.

removal of the tail and wing structures, removal of acoustic volumes behind bulkheads away from the crew and passenger compartment, and the removal of objects inside the cabin, such as trim, consoles, seats, and occupants.

The transfer function matrix **H** was populated using equations (4) and (5) for the LF portion up to 500 Hz. For the HF portion, expected RMS pressures within the interior obtained directly from SEA model solutions were included and artificial phase subsequently reintroduced per Equation 9. For each subsystem, the HF spectra were associated with points pertaining to the LF resolution within regions delimited by the subsystem extents, thus creating variations in the HF spectra corresponding to variations in the associated node areas within each subsystem. The mean and individual spectra of **H** associated with a side panel subsystem are plotted in Figure 4. Note that the acoustic coincidence frequency of the skins is approximately 5.5 kHz. At high frequencies, the statistical model of the interior driven by a pure tone assumes that the sound field can be modeled as sum of coherent plane waves with uniformly distributed random phases [11]. If considering the same subsystem shown in Figure 4 as an example, it is apparent in Figure 5 that the phase relationships of the transfer functions tend toward zero when averaged over many contributions, which corresponds to the average of the uniformly distributed reconstructed phase components of the HF spectra.

Simulated acoustic excitations from eight two-bladed rotors in a hover flight condition were then applied to the L+C UAM concept vehicle model. Note that structure-borne and turbulent boundary layer noise sources were not included, and the scattering effect of the fuselage on the excitation field was also not accounted for. Sound pressures from each of the eight rotors were propagated from each respective rotor center to 5762 points on the exterior vehicle surface and subsequently summed to form time domain excitations $x_m(t)$. The time history from each rotor included contributions from periodic tonal loading, blade thickness noise, and broadband self noise. The loading and blade thickness noise predictions were blade passage signals produced using Farassat's Formulation 1A [12, 13]. Self noise predictions were spectrally shaped noise time histories generated using the Brooks-Pope-Marcolini

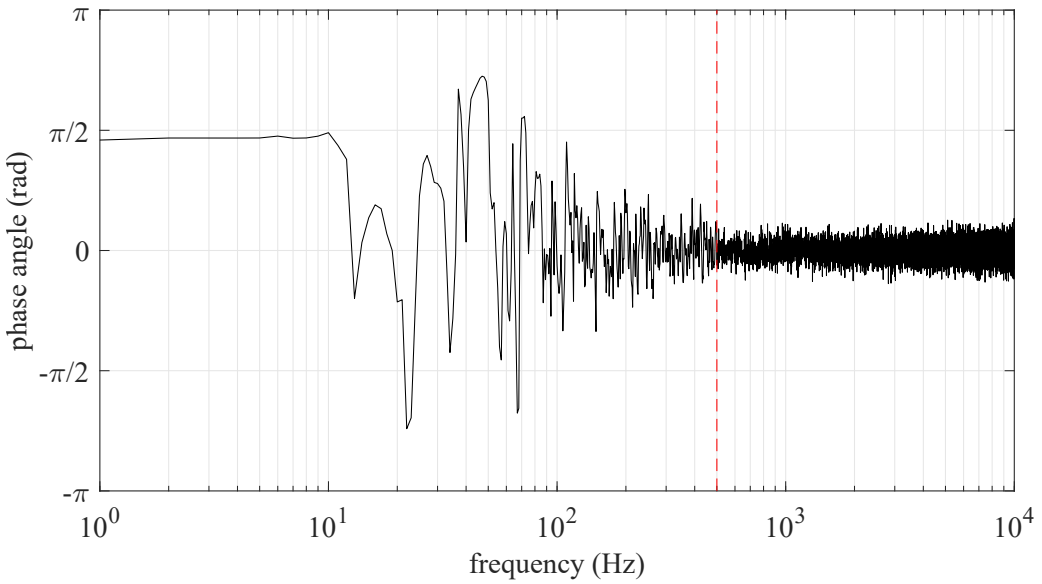

Figure 5: Mean value of the phase angles of the components of **H** shown in Figure 4.

self noise model in a rotating frame [14]. The blade geometry, blade passage frequency (35 Hz), loading, motion, inflow velocity, and effective angle of attack required to carry out the predictions were informed from the L+C concept and hover flight condition considered.

However, these predictions were not readily audible without further post-processing. The loading and thickness noise blade passage signals were too short, the self-noise predictions lacked phase information, and neither prediction was at a time resolution required for audio playback. To remedy this, the NASA Auralization Framework (NAF) was used to synthesize each rotor noise prediction into audible sound [15]. At each excitation point, the advanced NAF plugin for periodic additive sound synthesis extended the loading and thickness noise blade passage signal from each rotor to the auralization duration with the audio sample rate of 44.1 kHz. The NAF Modulated Broadband Synthesis Plugin [16] modulated a stochastic signal to generate the audible self noise. The NAF also was used to apply spherical spreading and atmospheric absorption effects (for uniform atmosphere at 15° C, 1 atm of pressure, and 70% relative humidity) to the synthesized sounds. Some approximations were made to reduce development and computation times associated with the generation of $x_m(t)$ for the purposes of exercising the hybrid auralization procedure. For example, short time histories (0.77 sec) were generated and subsequently repeated for listening purposes. Also, sounds were generated for a subset of the 5762 points and remaining time histories were populated using a magnitude and phase interpolation procedure.

Example pressure time histories sampled on the exterior and within the cabin interior are shown in Figure 6, and corresponding pressure spectra are shown in Figure 7. Most of the higher frequency broadband noise is filtered out by the vibroacoustic system, but the 35 Hz blade passage frequency is predominant in both plots and only slightly attenuated. This is in agreement with the sound characteristics perceived during audio playback.

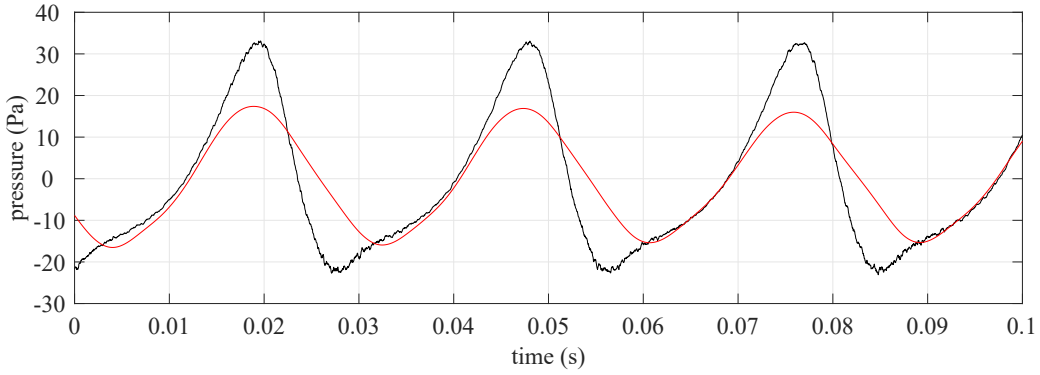

Figure 6: Simulated pressure time histories sampled on the windshield exterior (—) and cabin interior (—).

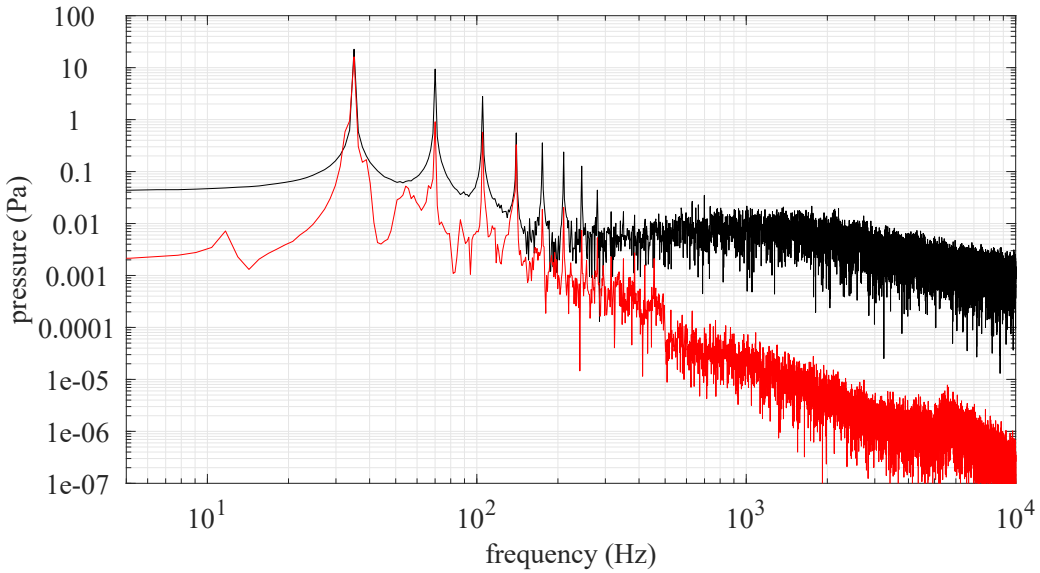

Figure 7: Simulated pressure spectra sampled on the windshield exterior (—) and cabin interior (—).

4. CONCLUSIONS

A procedure for auralizing interior noise that involves the creation of a hybrid LF/HF transfer function dataset for use with excitations such as exterior acoustic fields has been described and exercised on a UAM concept vehicle. With this approach, the amount of modeling and analysis can be adjusted depending on the use case, which can range from clientele demos to auralization studies used to inform product designs. For example, faster implementations may be realized by reducing the LF to HF transition frequency and applying simplifying assumptions to the model as was done here. On the other hand, higher fidelity auralizations could be obtained by specification of higher LF to HF transition frequencies, application of multiple excitation fields, and the use of FE direct steady-state dynamic solutions incorporating localized damping, interior trim details, etc. In light of this, further efforts focusing on additional noise sources, such as the turbulent boundary layer, drive train, and interior environmental control systems are of interest.

ACKNOWLEDGEMENTS

This work was funded by NASA's Aeronautics Research Mission Directorate through the RVLT Project. Vehicle geometry files were obtained from Justin Littell of the NASA LaRC Structural Dynamics Branch and Norma Farr from the NASA LaRC GEOLAB was instrumental in reconditioning the geometry for use in the analyses described here. Stefan Letica of the NASA LaRC Aeroacoustics Branch provided L+C vehicle rotor data used to generate acoustic predictions.

REFERENCES

[1] C. A. Powell and B. M. Sullivan. *Potential subjective effectiveness of active interior noise control in propeller airplanes*. TM-2000-210122, NASA Langley Research Center, 2000.

[2] C. Silva, W. Johnson, K. R. Antcliff, and M. D. Patterson. VTOL Urban Air Mobility concept vehicles for technology development. In *Proceedings of the 2018 Aviation Technology, Integration, and Operations Conference*, Atlanta, GA, June 2018.

[3] G. H. Koopman and H. F. Pollard. A joint acceptance function for enclosed spaces. *Journal of Sound and Vibration*, 73(3):429–446, 1980.

[4] R. H. Lyon and R. G. DeJong. *Theory and Application of Statistical Energy Analysis (2nd ed.)*. Butterworth-Heinemann, Newton, MA, 1995.

[5] J. E. Manning. Formulation of SEA parameters using mobility functions. *Philosophical Transactions of the Royal Society A*, 346:477–488, 1994.

[6] J. E. Manning. Hybrid SEA for mid-frequencies. In *Proceedings of the 2007 SAE Noise & Vibration Conference*, St. Charles, Illinois, May 2007.

[7] ESI Group. *VA ONE v1.17.0.1816*. www.esi-group.com. Rungis, France.

[8] R. V. Waterhouse. Interference patterns in reverberant sound fields. *Journal of the Acoustical Society of America*, 27(2):247–258, 1955.

[9] M. N. Ichchou, B. Hiverniau, and B. Troclet. Equivalent "rain on the roof" loads for random spatially correlated excitations in the mid-high frequency range. *Journal of Sound and Vibration*, 322:926–940, 2009.

[10] Dassault Systémes. *Abaqus CAE 2021.HF8*. www.3ds.com. Vélizy-Villacoublay, France.

[11] F. Jacobsen and P. M. Juhl. *Fundamentals of General Linear Acoustics*. John Wiley & Sons Ltd, West Sussex, UK, 2013.

[12] F. Farassat and G. P. Succi. A review of propeller discrete frequency noise prediction technology with emphasis on two current methods for time domain calculations. *Journal of Sound and Vibration*, 71(3):399–419, 1980.

[13] K. S. Brentner. *Prediction of helicopter rotor discrete frequency noise*. TM 87721, NASA Langley Research Center, 1986.

[14] T. F. Brooks, T. F. Pope, and M. A. Marcolini. *Airfoil self-noise and prediction*. RP-1218, NASA Langley Research Center, 1989.

[15] A. R. Aumann, B. C. Tuttle, W. L. Chapin, and S. A. Rizzi. The NASA Auralization Framework and plugin architecture. In *Proceedings of InterNoise 2015*, San Francisco, CA, 2015.

[16] S. Krishnamurthy, A. R. Aumann, and S. A. Rizzi. A synthesis plugin for auralization of rotor self noise. In *Proceedings of the AIAA Aviation Forum*, Virtual Event, 2021.